A Visualization Retrieval Framework for 3D Wheel Models with User-selected Geometric Features Regions

Dongliang Guo
Yanshan University

Lisha Zhou
Yanshan University

Jiaqi Zhang
Yanshan University

Ji Wang
CITIC Dicastal Co., Ltd.

Tianxiao Yuan
CITIC Dicastal Co., Ltd.

Yanfen Wang*
Yanshan University

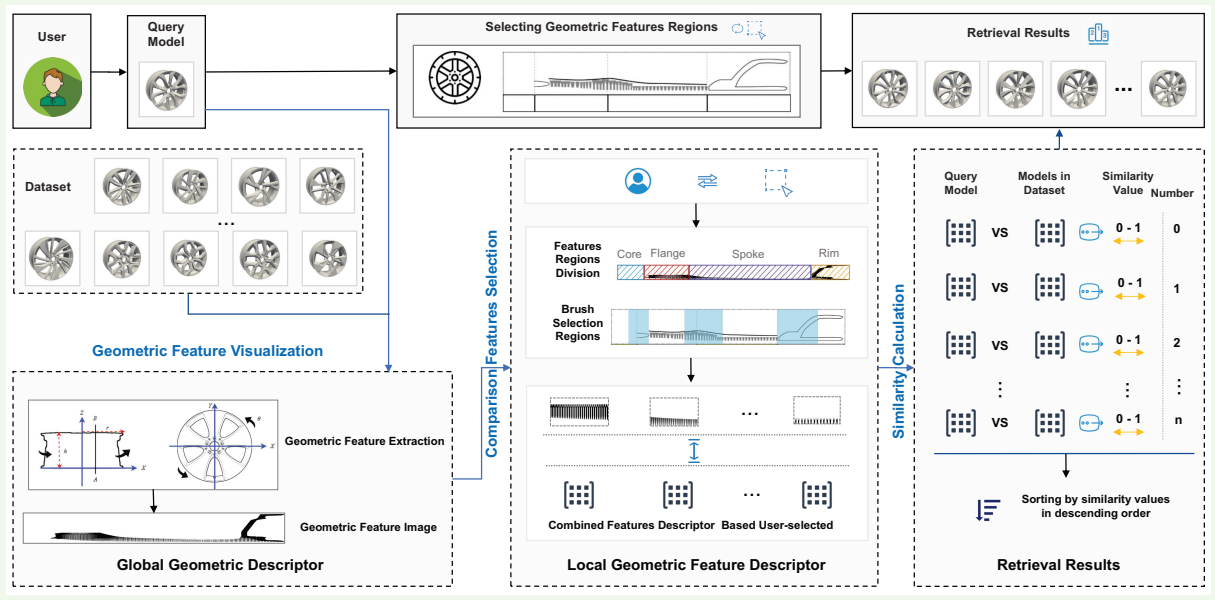

Figure 1: The Workflow of 3D Wheel Models Visualization Retrieval Framework. Initially, the geometric features of the 3D wheel models are visualized through preprocessing, resulting in 2D geometric feature images. Subsequently, based on the geometric feature regions selected by the user, these are transformed into combined feature descriptors for similarity calculation. Ultimately, the retrieval results are obtained by sorting the similarity values in descending order.

Abstract

Similarity retrieval of 3D product models is crucial for promoting the reuse of product design information and enhancing the production efficiency of enterprises. The 3D wheel models, widely used in industries such as automotive, railway, and aviation manufacturing, pose significant challenges in retrieval due to the high similarity between their global and local geometric features. This is because existing methods: (1) fail to effectively represent the geometric features of 3D wheel models, especially the local features that users focus on; (2) lack the flexibility in feature descriptors used for similarity calculation, making it difficult to accurately distinguish and match different models when dealing with highly similar local features. To address these problems, this paper proposes a visualization retrieval framework for 3D wheel models based on customizable geometric features regions. Firstly, a geometric feature extraction method is proposed that visualizes the geometric features of the 3D wheel models as binary geometric feature images, addressing the problem of representing both global and local geometric features. Secondly, building upon these geometric feature images, a customizable geometric features regions selection method is designed, enabling users to select multiple local geometric features to generate combined feature descriptors for similarity calculation in 3D wheel models retrieval. Finally, the effectiveness of the proposed framework is validated through experiments on industrial product datasets and user evaluations by domain experts, demonstrating its ability to promote the effective reuse of 3D wheel models product information.

Index Terms: Visualization retrieval, 3D model retrieval, 3D wheel models, geometric feature visualization, customizable regions selection.

1 Introduction

As a fundamental element of modern industrial manufacturing processes, 3D models of the product embed rich and highly valuable manufacturing information [1]. Statistical data indicates that 3D models are extensively reused in the design of new products [2]. Innovative designs represent only 25% of new products, while the remaining 75% are derived from the reuse or refinement of existing components [3]. 3D wheel models (3DWM) are extensively utilized in the automotive, railway, and aviation manufacturing industries, where they play an indispensable role. And the reuse of its information holds significant value. However, due to the high similarity in geometric features among related products, distinguishing between 3DWM using conventional retrieval methods proves to be particularly challenging [4]. Consequently, the development of ef-

*e-mail: wyf@ysu.edu.cn

ficient techniques for 3DWM retrieval, with the goal of enhancing information reuse efficiency, has emerged as a significant challenge in the current industrial manufacturing sector.

The content-based 3D model retrieval method has been shown to be effective [5, 6, 7, 8] . Among these, deep learning-based approaches have garnered extensive research attention due to their significant advantages in extracting both global and local features [9, 10, 11]. While these methods offer significant advantages in geometric feature extraction for 3DWM, several challenges remain when applying them in practical retrieval scenarios. Firstly, the process of representing geometric features is complex [12], making it difficult for users to understand the relationship between the retrieval results and the model features. This lack of comprehensibility can hinder the judgment of product information reuse. Secondly, these methods require large amounts of data for training[13], and the training process is both expensive and time-consuming. Lastly, although there is substantial research on visual neural networks that supports experimentation and fine-tuning for deep learning techniques [14, 15], this process can be a costly learning task for users in industrial design scenarios.

In product design, designers' retrieval requirements for 3DWM go beyond global-level matching. They frequently need to retrieve local geometric features and detailed local features within highly similar local structures. However, existing methods primarily focus on global feature matching and no selectivity, which is insufficient for meeting the high-frequency demands for local feature retrieval in industrial design contexts. This limitation prevents designers from fully utilizing the design resource information in the existing product library, thereby affecting the efficiency and quality of product development.

In order to tackle the previously discussed challenges,this paper proposes a visual retrieval framework for 3DWM. The starting point is to visualize 3DWM's geometric features into binary geometric feature images, where 3D geometric features are mapped onto 2D geometric shapes. This geometric feature image can simultaneously represent both global and local features while maintaining significant intelligibility. Building upon this, we design a geometric feature region segmentation and interaction strategy, which enables users to customize the region of interest in geometric feature images as combining feature descriptors. The combining feature descriptors to achieve multi feature similarity calculation in 3DWM. The main contributions of this paper are as follows:

- **A method for extracting geometric features in 3DWM.** This method maps the subtle concave convex structures of the model to binary images through axial rotation scanning algorithm, generating understandable and easily comparable 3DWM geometric feature images. And it has good robustness, does not rely on data training, and can ensure the stability and accuracy of feature extraction.

- **A method for dividing geometric feature regions and combining features.** This method firstly divides the geometric feature image of the 3DWM into four feature regions based on the needs of domain experts: core, flange, spoke, and rim. Secondly, it designs a multi-local feature retrieval scheme that combines geometric feature images with custom selected regions and segmented features. Constructing composite feature descriptors for similarity calculation through customizable selection can improve the accuracy of 3DWM retrieval.

- **Evaluation of retrieval framework.** Through the analysis of the experimental results of retrieval on industrial product data sets and the user evaluation of domain experts, we verify its effectiveness in 3DWM retrieval.

2 Related Work

In this section, we provide a review of the existing 3D model retrieval, global geometric feature descriptor and local geometric feature descriptor.

2.1 3D Model Retrieval

3D model retrieval has consistently been a prominent region of research attention among scholars [14, 15]. Driven by application scenarios, the initial 3D model retrieval task aims to retrieve models of the same category from a large number of different classes [16, 17, 18]. This greatly improves the management efficiency of the large number of 3D models generated with the advancement of CAD/CAE technology. However, as product manufacturing and industry development have become increasingly refined, 3D model retrieval tasks have gradually evolved to address finer grained goals, such as product part assembly retrieval and product design feature retrieval [19, 20]. This indicates that through the combination of theoretical research and practical experiments, fine-grained 3D model retrieval [21, 22] is more suitable for meeting the growing demand for more accurate and professional retrieval tasks in application scenarios.

3D model retrieval methods can be classified based on the types of data features they rely on, primarily including text-based and content-based methods. The text-based retrieval methods [23] offers advantages in terms of simplicity and computational efficiency, as it matches descriptive text or labels associated with the models, making it particularly suitable for model libraries with well-defined annotations. However, it is highly dependent on the accuracy and completeness of the text annotations, and its retrieval performance tends to degrade when models lack sufficient descriptions or contain inaccurate labels. In contrast, content-based retrieval methods [24] focus on analyzing the intrinsic features of the models, such as geometric shape, structure, and texture, enabling more precise matching by circumventing the need for text labels. The content-based retrieval methods better captures the actual characteristics of the models, particularly in scenarios where text annotations are inadequate or absent, thus offering significant advantages in such cases.

2.2 Global Geometric Feature Descriptor

Content-based retrieval techniques for 3D models primarily focus on the physical attributes of the models, enabling model similarity retrieval through the extraction and analysis of geometric features, topology, and other physical properties.

Osada et al. [25] introduced the concept of shape distribution, pioneering a method that represents the geometric properties of 3D shapes as statistical histograms. he shape matching problem is reduced to a comparison of probability distributions, enabling 3D model retrieval based on statistical features. This approach offers the advantages of computational simplicity and insensitivity to the model's representation form. However, it also faces limitations, particularly its insensitivity to the local details of the model. To address the limitations of shape distribution methods, researchers have proposed various enhancement strategies[26, 27, 28]. While these methods improve the accuracy of feature description to some extent, the histogram vectors remain highly sensitive to transformations that significantly impact the model's surface, such as Gaussian noise interference and mesh simplification, which in turn reduces retrieval efficiency. To further enhance the robustness of feature representation, Vranic et al. [29] first proposed a model retrieval method based on spherical harmonic functions. Building upon this foundation, subsequent research has further refined the ball-harmonic function-based method by incorporating more complex transforms or functions to improve performance, such as the modified ball-harmonic function [30], the ball-harmonic entropy function [31], and the ellipsoidal ball-harmonic function [32], among

others. However, the ball-harmonic projection relies on global expansion, which makes it challenging to effectively capture local features (e.g., small protrusions or depressions). As a result, it may lead to the misclassification of locally distinct models as similar, thereby compromising retrieval accuracy. To represent the topology of 3D models, Hilaga et al. [33] proposed a multi-resolution Reeb image that captures the topology of 3D models at different levels of resolution. While Reeb images provide a stable representation of topology across different resolutions, they lack the ability to distinguish between distinct parts of the model. In contrast, Sirin et al. [34] proposed a skeleton fill-rate-based retrieval method for both 2D and 3D models. By comparing the skeleton fill rates of different models, the method facilitates effective model retrieval. Although both the Reeb image and skeleton map-based methods can effectively differentiate between primary and secondary structures within 3D models, they still face challenges in accurately deconstructing 3D models, with the deconstruction process being sensitive to model noise.

With the rapid development of deep learning, numerous new approaches have emerged in the field of 3D model retrieval. These methods can extract the geometric features of 3D models more comprehensively and can be classified into four categories based on their feature representation: voxel-based methods [35], point-cloud-based methods[41], view-based methods[36], and B-rep-based methods [37]. Wu et al. [38] proposed a neural network model called 3D ShapeNets, which is based on a Deep Belief Network (DBN) [39]. They designed a Convolutional Deep Belief Network (CDBN) to represent the 3D model as a probability distribution of binary variables on a voxel grid, allowing for feature extraction directly from the voxel-represented 3D grid. Qi et al. [41] developed the PointNet model, which can directly process disordered point cloud data and perform feature extraction and global feature fusion through a multi-layer network structure. Su et al. [42] presented the MVCNN network, which projects the 3D model into multiple 2D views, then uses a convolutional neural network to extract features from each view. The multiple view features are subsequently fused via a maximum pooling operation to generate a global descriptor for model retrieval. Methods such as [43, 44, 45] have built upon MVCNN, achieving improved retrieval results through continuous innovations and optimizations in the view projection and convolution methods. However, view-based approaches still struggle with unifying the description of the internal and external features of objects. To address this limitation, Lin et al. [40] developed the 3D Orthogonal Integral Transform (OIT), which consists of three separate integrals in orthogonal planes that are rotated to cover all directions, allowing for a more comprehensive description of the geometric features of 3D models. Retrieval methods based on voxels, point clouds, and views often focus primarily on the geometric shape of 3D models, underutilizing topological information. To resolve this issue, several deep learning-based retrieval methods leveraging B-rep representations have emerged in recent years. Colligan et al. [46] proposed an innovative 3D shape representation method based on the B-rep model, enabling the learning of both the surface geometry and topology of a CAD model. Additionally, Hierarchical CADNet, a hierarchical graph convolutional network, learns the hierarchical structures of B-rep graphs. Hou et al. [47] transformed B-rep data into a shape descriptor known as a B-rep graph and applied a graph pooling (FuSPool) algorithm on graph convolutional networks (GCNs). They developed FuS-GCN, a new neural network for aggregating topological and geometric features, effectively learning global 3D-CAD shape descriptors.

The retrieval of 3DWM, like other types of 3D model retrieval, faces several challenges when using deep learning methods. Firstly, these methods require large amounts of data to train a pre-trained model for feature extraction, but in some product application scenarios, users are unable to provide such large datasets. Secondly, deep learning models are often treated as 'black boxes', which makes the feature extraction process less interpretable. The lack of interpretability hinders users from understanding the logic behind the retrieval results, which may pose limitations in applications that require high levels of transparency. In contrast, we propose using geometric feature images as descriptors to represent the geometric features of 3DWM, a method that does not rely on data training. This method enhances robustness and interpretability, enabling users to better understand the relationship between geometric features and similarity retrieval results.

2.3 Local Geometric Feature Descriptor

Most existing 3D model retrieval methods focus on global shape features, which compare overall shape similarity. However, as designers increasingly require the ability to locate and modify specific local structures within model libraries, recent methods have emerged that emphasize local feature-based retrieval to better address these needs.

Among the local feature-based retrieval methods, two representative approaches are proposed in the literature [48, 49]. The method presented in [48] enables local structure retrieval by constructing multi-scale feature representations using scale space techniques. This approach first extracts the local features of the model at various scales, organizes these features into a binary tree structure, and ultimately performs similarity comparison of the local structures through a subgraph matching algorithm. In contrast, [49] extends the Reeb graph, which represents the topology of the 3D model as a graph structure, and uses graph matching techniques to achieve local feature retrieval. While these two methods theoretically allow for local structure retrieval, they present several notable drawbacks in practical applications: first, the computational complexity involved in constructing and matching subgraphs is high and time-consuming; second, the recognition accuracy of local features is low when dealing with complex industrial models [19], which makes them unsuitable for meeting the demands of practical industrial applications.

To address the above problems, Bai et al. [50] proposed a local structure retrieval method for 3D models based on DBMS graphs (multi-resolution skeleton graphs) and subgraph matching. This method constructs a hierarchical graph structure representation by extracting multi-resolution skeleton features from the model and utilizes an improved subgraph matching algorithm for local structure retrieval. While this approach enhances retrieval efficiency to some extent, it still suffers from high computational complexity and is sensitive to model noise, which limits its applicability to real industrial data.

On the other hand, methods based on B-rep (boundary representation) model segmentation are also commonly employed for sub-part retrieval. These methods first utilize the geometric and topological information of the model to decompose it into a set of parts, then classify and extract features from these parts, and finally use these features for part retrieval. Jayaraman et al. [52] proposed an innovative approach to represent the geometric features of the model by using the U- and V-parameter domains of the curves and surfaces, and constructing an adjacency graph to represent the topology of the model. Building on this representation, they introduced the UV-Net architecture, which combines an image-based convolutional neural network (CNN) and a hierarchical graph neural network (GNN). This approach demonstrates strong performance in both supervised and unsupervised tasks across multiple datasets, surpassing other 3D model retrieval methods. However, UV-Net also has its limitations: while it performs well on labeled datasets, its model training currently relies exclusively on labeled data and cannot be directly applied to unlabeled datasets, which restricts its applicability in broader scenarios.

Compared to other class models, 3DWM exhibits more detailed

features, which makes the retrieval of local features more challenging. Guided by user needs in practical application scenarios, this paper proposes an innovative visual interactive retrieval framework to overcome the limitations of existing local feature retrieval methods of 3DWM. Firstly, the framework is user-centered, allowing users to freely configure local feature descriptors and providing flexible customization for local feature description and retrieval. Secondly, it eliminates the need for labeling unlabeled data, enabling direct application to unlabeled datasets, thereby significantly expanding the scope of the method's applicability.

3 METHODOLOGY

3.1 Workflow of Framwork

Our work is driven by the needs of industrial designers. Product design experts within the enterprise aim to identify a method for geometric feature representation and retrieval that supports 3DWM, without relying on large-scale data training. Through close collaboration with these experts (**D1**, **D2**, **D3**, **D4**, **D5**), and drawing from existing literature as well as multiple iterative participatory meetings, we have identified three core tasks for the visualization retrieval frameworks of 3DWM:

T1: *Utilize visual, graphical geometric feature characterization to help the user distinguish local features among similar 3DWM.* Without the need for training data, the image represented by the geometric features allows for the observation of local feature differences in highly similar 3DWM, further supporting the comparison of similarity.

T2: *Support interactive, user-centered selection of local geometric features based on geometric representation.* The selection of local geometric feature regions should cater to users' frequent need for comparing multiple local features, and the relationship between feature descriptors and retrieval results should be easily interpretable.

T3: *Ensure that similarity calculation is comprehensible within the context of the geometric feature images and interactive retrieval framework.* The similarity calculation method should establish a clear connection between geometric features and the retrieval results of 3DWM, enabling users to gain an intuitive understanding of the features and facilitating the full exploitation of the retrieval results.

The framework based on the requirements proposed in this paper is illustrated in Fig.1, consisting of three key modules: geometric features visualization, interactive multi-local geometric features selection, and similarity calculation. The shape descriptor of the 3DWM is comprised of two primary components: global geometric feature and multi-local geometric features. Firstly, the 3D geometric features of the 3DWM are visualized as 2D images, from which global geometric feature descriptor is constructed. The global geometric feature descriptor is designed to effectively distinguish local geometric features of similar models. Then, the geometric feature image of 3DWM is divided into four key design regions: the core, flange, spoke, and hub. Using interactive visualization, customizable local geometric feature descriptors are developed to efficiently characterize retrieval features. Finally, a flexible similarity calculation method, based on geometric image features and descriptor features, is proprosed to enhance the precision and accuracy of retrieval results.

3.2 Geometric Feature Visualization

Based on **T1**, it showed that the user expects to intuitively establish a relationship between the 3D geometric features of the 3DWM and the geometric features used for similarity calculation, without relying on complex feature extraction and representation methods. Additionally, the user seeks to effectively observe local geometric feature differences between similar models. In response to this, we design a content-based method to visualize the 3DWM's geometric features as 2D images. These 2D images allow users to clearly observe the key design features and local details of the 3DWM, thereby better understanding the feature descriptors for 3D model retrieval. First, we extract the geometric features of the 3DWM by designing moved line segments and axially rotated model intersect, which encompass internal grooves, facets, and other intricate details. Then, the generated intersection points are mapped onto a 2D plane to produce geometric feature images, which serve as visual descriptors for the geometric features of 3DWM. The geometric feature images generated by this algorithm can capture multiple key dimensional aspects of 3DWM, including, but not limited to, surface texture, thickness, and shape, thereby offering a more comprehensive and accurate representation of geometric features.

The 3DWM geometric feature visualization process is shown in Fig. 2. Specifically, a line segment intersector AB is first set up at the axial position of the 3DWM along the Z-axis direction and sampled according to the pre-set parameters. Fig. 2 (a) shows the schematic diagram of feature extraction of the wheel model in the 3D scene, and Fig.2 (b) shows the feature image after feature extraction and mapping. In Fig. 2, AB is the line intersector, r is the radius of the bottom surface of the 3DWM, h is the maximum height of the 3DWM, and θ is the axial step (counterclockwise) angle.

The specific steps of the feature extraction algorithm are outlined in Algorithm 1. Initially, a line segment intersector AB is created at the axial center of the 3DWM. This line segment is then progressively moved along the X-axis towards the edge of the 3DWM, with the movement governed by the set radial step distance d. At each step, the 3DWM is rotated counterclockwise around the Z-axis by the axial step angle θ. During this process, the line intersector AB collides with the 3DWM,generating an even number of collision points. Two pairs of these points are of particular : one where the line intersector penetrates the 3DWM (penetration point), and one where it exits (exit point). By calculating the coordinates of these collision points, the thickness of the 3DWM at the current location can be determined. Specifically, the thickness distribution of the 3DWM along the Z-axis is obtained by utilizing the difference in the coordinates of the penetration and exit points. Using this spiral sampling method, the spatial structural characteristics of the 3DWM in the XoY plane can be extracted.

After calculating the thickness information from the difference between the penetration and exit points, the data must be scaled and mapped into the geometric feature image. Specifically, the thickness value at each sampling point is mapped to the corresponding position on the feature image based on its location in the XoY plane and its height along the Z-axis. In the geometric feature image (Fig. 2(c)), both solid and insubstantial information at each

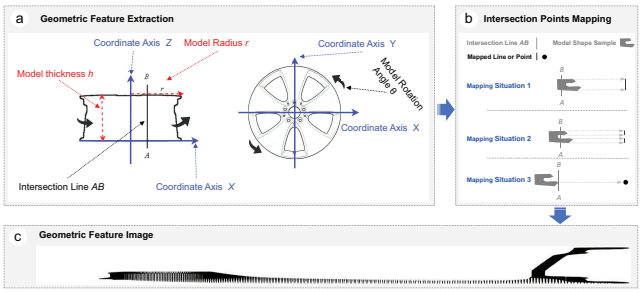

Fig. 2 The Process of Visualizing the Geometric Features of 3DWM into 2D Geometric Feature Images.

Algorithm 1 Geometric Feature Extraction Algorithm

Require: Radial 3D model M, radial unit step length d, axial unit step (counterclockwise) angle θ, geometric feature map of M with width and height m and n pixels
Ensure: geometric feature map $P_{m\times n}$ of M

Compute the columnar envelope M^* of M
Calculate the bottom radius r and height h of M^*
Construct a coordinate system with the bottom center of M^* as the origin of the Cartesian coordinate system, where the XY axis is located on the bottom of M^* and the Z-axis points to the top center of M^*
Define the line segment AB that overlaps the Z-axis, where the coordinates of A are $(0,0,-0.1h)$ and the coordinates of B are $(0,0,1.1h)$
$i \Leftarrow 0$
while $A_x < r$ and $i < m$ **do**
    Calculate the set $F \Leftarrow \{C_0D_0, C_1D_1, C_2D_2 \cdots\}$ of line segments AB intersecting the 3D model M
    $j \Leftarrow 0$
    while $j < n$ **do**
        if $j \times (h/(n-1))$ is located on any intersection segment C_xD_x of F **then**
            $P_{ij} \Leftarrow 1$
        else
            $P_{ij} \Leftarrow 0$
        end if
        $j \Leftarrow j+1$
    end while
    $i \Leftarrow i+1$
    $M \Leftarrow Rotate(M, \theta, Z)$
    $A \Leftarrow A + (i \times (r/(m-1)), 0, -0.1h)$
    $B \Leftarrow B + (i \times (r/(m-1)), 0, 1.1h)$
end while

sampling point are represented by different values, resulting in a two-dimensional image that reflects the thickness distribution of the 3DWM. This process allows for the accurate representation of the spatial structure and geometric features of the 3DWM in the feature image.

In the proposed geometric feature extraction algorithm, the parameter settings are crucial for both the effectiveness of geometric feature visualization and the performance of the algorithm. The following key parameters are primarily considered: the 3DWM rotation angle θ, the intersection line step size d, and the width m and height n of the geometric feature image. These parameters are designed based on the practical retrieval requirements. First, regarding the rotation angle θ of the 3DWM, we conducted experiments to compare the density of intersection line sampling for angles ranging from 1 to 2 degrees. Based on the results, a rotation angle of 1.8 degrees was selected, which is equivalent to sampling 200 times for each complete rotation (360 degrees). Second, since uniform sampling better represents the geometric features of the 3DWM, we further compared different values for the width and height of the geometric feature image to assess their ability to capture the fine details of the 3DWM's geometry shape. After testing, we set $m = 20000$ and $n = 300$, with the intersection line step size $d = xMax/20000$, where $xMax$ represents the maximum value in the X direction of the model's bounding box. It is important to note that both the visualization of geometric features and the similarity calculation are influenced by the initial rotation angle of the 3DWM. To minimize the bias caused by this effect, we manually adjusted the initial rotation angle for all models between feature extraction steps.

Overall, this feature extraction method based on rotary sampling effectively captures both the surface features of the 3DWM and its internal concave and convex structures. It accurately extracts the structural information of the wheel through the calculation of multiple collision points, which are then mapped into a binarized feature image, providing a reliable data foundation for subsequent analysis and processing.

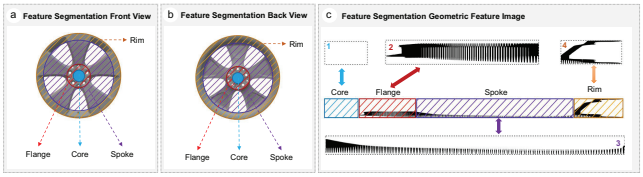

Fig. 3 Geometric Feature Image Region Division. (a), (b) and (c) show the positions of the core, flange, spoke, and rim corresponding to the segmentation of the model's front and back views and geometric feature images. (1),(2),(3), and (4) are segmented images of the geometric feature images.

3.3 Interactive Multi-local Geometric Features Selection

Based on **T2**, users require a method to customize local multi-features for input, in order to meet the frequent and diverse feature retrieval needs in design application scenarios. To address this challenge, we propose a retrieval method based on user-selected regions and segmented features from geometric feature images. First, the geometric feature image is divided into segments according to the geometric regions of the 3DWM, creating segmented feature regions. An interactive selection interface is then provided, allowing users to customize the regions of the geometric feature image. Finally, the user's selected regions are integrated into a combined feature descriptor. The following two sections provide a detailed explanation of the proposed approach.

3.3.1 Geometric Feature Segmentation

According to the distinct concave and convex structures of each segmented part of the 3DWM mapped in the feature image, we designed a component segmentation method generalized to the 3DWM by taking advantage of the 3DWM's cartographic structure. The method can accurately subdivide the geometric feature image of the 3DWM into four parts: core, flange, spoke and rim, and the specific division is shown in Fig. 3. Prior to feature image segmentation, the binarized feature image is first transformed into a two-dimensional matrix $P \in \{0,1\}^{m\times n}$. Here, m represents the number of rows in the matrix, corresponding to the number of pixel elements along the rows of the image, and n represents the number of columns in the matrix, corresponding to the number of pixel elements along the columns of the image. Using Equations 1, 2, and 3, three segmentation points, $k1$, $k2$, and $k3$, can be obtained. k_1 (Equation 1)is the geometric feature image segmentation points of 3DWM core and flange.

$$k_1 = min\left\{ j | \sum_{i=1}^{n} P_{ij} > 0 \right\} \tag{1}$$

where, since the core portion of the 3DWM is completely blank and devoid of any entities, the first column in which an entity appears is the starting position of the flange. By summing the feature image columns, the first non-zero column indicates the split point between the core and the flange. k_2 (Equation 2) represents the segmentation points of the 3DWM flange and spoke in the geometric feature image.

$$k_2 = \min\left\{ j | P_{i,j} = 1 \wedge P_{i,j+1} = 0, j \in \left\{ 1, 2, ..., \frac{m}{2} \right\} \right\} \tag{2}$$

The split point between the flange and the spoke is identified as the highest point in the first half of the feature image. As shown in the geometric feature extraction plot, as the line intersector moves outward along the X-axis in the flange region, the flange's thickness gradually increases until it reaches the junction with the spoke, where both the thickness and the height reach their maximum values. Therefore, in this method, by traversing the rows of the matrix P (representing the height of the feature image) and the columns of P (representing the width of the feature image), the first non-zero point is identified as the highest point of the feature image. The equation constrains the range of values of the columns to ensure that the division point is located in the first half of the feature image. k_3 (Equation 3) represents the segmentation points between the 3DWM core and flange in the geometric feature image.

$$k_3 = \frac{m}{2} + min\left\{ j | \sum_{i=1}^{\frac{2n}{3}} P_{i,\frac{m}{2}+j} > 0 \right\} \tag{3}$$

As show in Fig. 3, in the second half of the image, the height of the spoke part is lower, while the height of the rim part is significantly higher. Therefore, the point at which the spokes are divided from the rim is determined by summing the matrix in columns at 2/3 of the height from top to bottom of the second half of the feature image. In the summation matrix, there is no entity in the spoke portion of the 3DWM until there is an entity in the rim portion of the wheel. Therefore, the column coordinates of the first non-zero point of the summation matrix are chosen as the split point between the spoke and the rim.

3.3.2 User-selected Geometric Features Regions Interaction Method

Building upon the segmented design of geometric features, we have further developed a feature retrieval interaction scheme, as illustrated in Fig. 4. This interaction design is composed of four components: the feature segmentation selection region(Fig. 4(c)), the custom feature selection region(Fig. 4(b)), the wheel schematic diagram(Fig. 4(a)), and the data prompt region(Fig. 4(d)). The feature segmentation selection region is organized according to the four main components of the wheel: the wheel core, rim, spokes, and flange. A block selection button is provided to offer users quick access to feature selection options. Additionally, a concentric feature interaction design with the left wheel shape is incorporated to enhance the user's perception of the retrieved features. The custom feature selection region is designed designed as a self-directed brushing zone with a shape display, enabling users to select regions based on specific local features as needed. For example, users can select features from the flange hole region or the spoke shape section for retrieval. The wheel schematic diagram serves as both a design example and background image of the wheel. It is based on the concentric arrangement of the front view of the wheel core, rim, spokes, and other key components, and is designed to interact with the user's selections in the segmented selection region on the right, providing an interactive display. The data prompt region assists users in selecting the current feature data. The starting and ending positions of each feature region are marked as 0 and 1, respectively, and the regions selected by the user are mapped to proportional data displays according to their corresponding relationships.

It is important to note that the similarity of design features is not based on a single feature; rather, users need to search for multiple features, such as flange similarity and spoke fork similarity. To address this, we combine the feature segmentation selection region with the custom feature selection region. By simultaneously selecting features from both regions, a combined feature descriptor is created for retrieval.

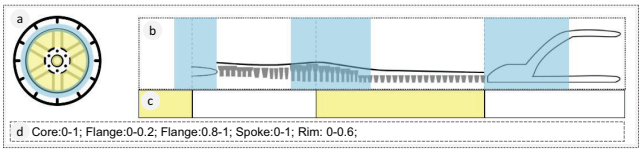

Fig. 4 Interactive Design for Users to Select Geometric Feature Regions. (a) is the wheel schematic diagram. (b) is the custom feature selection region. (c) is the feature segmentation selection region. (d) is the data prompt region.

3.4 Similarity Calculation

Based on **T3**, and in conjunction with **T1** and **T2**, it is evident that the similarity calculation method serves as a crucial foundation for ranking 3DWM retrieval results. It plays a key role in helping users understand the correlation between the retrieval results and the retrieval features. A higher similarity value between the query model and the comparison model indicates a greater degree of similarity between the two models. We propose a variable similarity calculation method based on the combination of feature descriptors which are flexibly selected by users. If the geometric feature descriptor is a single-feature segmented descriptor, the XOR method is applied to calculate the similarity between the geometric feature images. In the case of a combined descriptor consisting of multiple feature regions, the XOR method is first used to calculate the similarity of the geometric feature segmentation maps within the selected regions. Subsequently, the importance of each selected region is assessed, and the weighted ratios of the different selection regions are aggregated into a total ratio for calculating the overall similarity. The weighting rule is multiplying the similarity ratio of each selection by the ratio of the length of the selection in the X direction to the total length of the user's selection in the X direction. The weighting strategy for the combined features is based on the segmented features, thereby ensuring the consistency of the weighting rules when calculating the regions selected by the user.

Specifically, as outlined in Algorithm 2, the process begins by determining the geometric feature map to be compared for region segmentation based on the scale range selected by the user. For the wheel core, which lacks a physical entity, the length of the feature map is directly compared to calculate similarity. For the three more complex structural components—the flange, spoke, and rim—the XOR operation is applied to the corresponding images to compute the similarity ratio. It is important to note that the XOR method is specifically chosen over the AND method, as XOR can more comprehensively capture the spatial feature information of the model, including the features of non-solid parts such as bolt holes, spoke gaps, and others. These features are critical for accurately identifying the wheel model. To ensure the accuracy of the feature comparison, the algorithm incorporates a weighting ratio. Specifically, the similarity ratio of each component is multiplied by the ratio of the component's length in the direction of comparison to the total length of the user's selected region in the same direction. This allows for a comprehensive assessment of the influence of different feature regions on the final similarity result. All weighted ratios are then aggregated to produce a final total similarity ratio. Finally, the algorithm ranks all results in descending order based on similarity, outputting the calculated similarity results.

A point to consider is that the segmented feature region images obtained in Section 3.3.1 are variable-length sequences, as the width m of the images is not exactly the same. This is due to the different sizes of the 3DWM models. However, since the size differences in the 3DWM wheels are within a certain range, a truncation strategy is adopted for the similarity calculation between images with different widths. Specifically, when comparing the similarity between two images with different widths m, the image with the

Algorithm 2 Similarity Calculation Algorithm

Require: Geometric feature images Wheel core atlas D_1, Flange atlas D_2, Spoke atlas D_3, Rim atlas D_4, each with c objects, respectively, a query model user-defined constituency set T of width and height $m_k \times n_k$ contains d data instances that are scaled to the query model geometric feature image according to an array of constituency proportions sent to the algorithm by the interactive selection, where $m_k = \left|x_k^* - x_k\right|$, x_k is the minimum value of the kth selection on the X-axis, x_k^* is the maximum value of the selection on the X-axis, and n_k is the Y-axis value of the selection image.

Ensure: The similarity retrieval result set $R = \{a_n, b_n\}$, where a_n is the wheel model ID and b_n is the similarity ratio between the wheel and the retrieved wheel.

$i \Leftarrow 0$
while $i < c$ **do**
  $j \Leftarrow 0$
  Wheel similarity ratio $b_i \Leftarrow 0$
  while $j < d$ **do**
    Divide the geometric feature image of the corresponding atlas according to the proportion in T_j (divided into D_{1i} or D_{2i}, D_{3i}, D_{4i})
    if The T_j selection is located in the core of the wheel **then**
      $b_j \Leftarrow \frac{T_j}{D_{1i}}$
    else
      Compare the feature image pixel points of T_j and D_{2i} (or D_{3i}, D_{4i}) in the flange (or spoke, wheel rim) image set using exclusive XOR method to calculate the similarity ratio b_j
    end if
    $b_i \Leftarrow b_i + b_j \times \frac{m_j}{\sum_{k=0}^{d-1} m_k}$
    $j \Leftarrow j + 1$
  end while
  $R \Leftarrow (a_i, b_i)$
  $i \Leftarrow i + 1$
end while
Sort R in ascending order based on b_n **return** R

wider width is truncated to match the width of the other image.

4 Experiment and User Evaluation

4.1 Experiment on Wheel Dataset

4.1.1 Dataset Construction and Initialization

The work presented in this paper focuses on inter-class similarity retrieval for automotive wheels. The dataset utilized should consist of CAD models of automotive wheels with consistent design specifications. However, among the existing publicly available CAD model repositories (e.g., the ESB model repository [53], the CadNet40 database [47], and the DMUNet database [54]), there is a scarcity of high-precision 3D CAD models specifically designed for automotive wheels.

We construct a 3DWM dataset based on the STEP standard in collaboration with wheel manufacturing enterprises. This dataset is derived from real-world design cases provided by these enterprises, and the models are anonymized to ensure their accuracy and applicability for experimental purposes. Through discussions with industry experts, 105 representative 3DWM are selected, encompassing a diverse range of wheel design styles and specifications. Additionally, we assign a numbering system to the model set (starting with 'W' and numbered sequentially from 1 to 105) and extract both front and side views of the models for the presentation and evaluation of retrieval results.

4.1.2 Global Geometric Feature Retrieval Comparison

To verify the effectiveness of our method in global geometric feature retrieval, we compare it with the approaches Fourier Descriptors [51] and the proposed in UV-Net [52]. Fourier descriptors can maintain the invariance of rotation, scaling, and reflection, making them highly suitable for shape matching. The UV-Net in enhances feature robustness and retrieval accuracy by mapping the geometric features of each face of the model to a two-dimensional mesh composed of curves and surfaces, and connecting them through adjacency graphs. In contrast, the geometric feature extraction method proposed in this paper analyzes the model's surface structure, extracts key features, and maps them to a two-dimensional image. These methods are capable of incorporating both global and local information, making them suitable for a comparative analysis of retrieval performance.

Fourier Descriptors Method: Project the spoke surface of the model onto a 3D plane, compute Fourier descriptors, and measure the similarity between models using cosine similarity.

UV-Net Method: First, using the network architecture and training parameters provided by the UV-Net model, we obtained 512-dimensional high-dimensional feature vectors for each 3DWM. Next, a similarity measurement criterion was established based on the Euclidean distance between feature vectors, and the retrieval results were computed.

To ensure the fairness of the comparative experiment, the retrieval results are visualized in descending order of similarity, with similarity decreasing from left to right.

The retrieval results of three methods for the same wheel model are shown in Fig. 5. In these results, the model most similar to the query is ranked first, with the similarity decreasing as the ranking position moves lower. During the experiment, two wheel models with distinct designs were selected as query samples: one with a large number of spokes and a complex structure, and the other with fewer spokes and a simpler structure. This selection ensured a comprehensive validation of the method. In the retrieval results, model numbers that differ significantly from the query model are highlighted in red and bold. These differences primarily reflect mismatches in the number of spokes and flange structure (e.g., the number of flange holes) when compared to the query model.

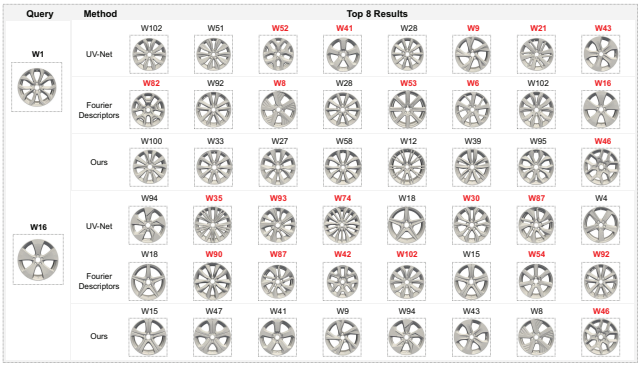

Fig. 5 Comparison of Our Method with the Global Feature Retrieval Results of Fourier Descriptors [51] and UV-Net [52]. Models in the search results that exhibit significant differences from the query model are highlighted in red and bold. The main differences include variations in the number of spokes and the flange structure compared to the query model.

Through comparative analysis, it can be observed that, for both the complex model W1 and the simpler model W16, the models retrieved using our proposed method exhibit a high degree of similarity to the query model in terms of wheel structure. Although

some models with differing spoke numbers appear in the retrieval results, they are not ranked highly. In contrast, models retrieved using the UV-Net method often show significant structural differences from the query model. The Fourier descriptors method yields the worst results, with the lowest similarity in model structure and features. Therefore, in terms of the visualization of retrieval results and the degree of alignment with the actual wheel structure, our method outperforms Fourier descriptor and UV-Net.

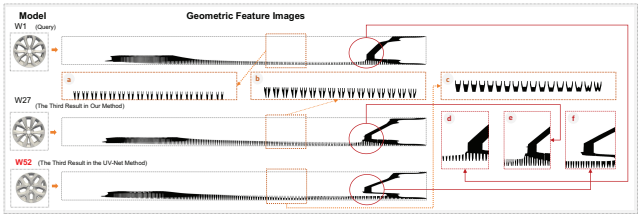

Fig. 6 Comparison Between the the Geometric Feature Images of W1, W27, and W52. (a), (b), and (c) are enlarged images of each red rectangular box. (d), (e), and (f) are enlarged images of each circular box.

Fig. 5 shows that the structure of the third model (W52) in the UV-Net method differs significantly from that of W1, while the structure of W27 in our method is closer to that of W1. We compare the geometric feature images of models W1, W52, and W27 (shown in Fig. 6). It is evident that the serrated structure of the spoke section in the zoomed-in local image of the geometric feature of model W52 (Fig. 6(c)) differs significantly from the serrated structure of the query model W1 (Fig. 6(a)). In contrast, the W27 model retrieved using our method (Fig. 6(b)) is more consistent with W1. Additionally, the red ellipse in the rim feature image of the W52 model appears blank (Fig. 6(f)), whereas the corresponding structure in W27 (Fig. 6(e)) is more similar to that of W1 in the same region (Fig. 6(d)). This further demonstrates that the geometric feature images extracted by our method effectively represent the model's geometric characteristics and offer better interpretability.

4.1.3 Interactive Feature Evaluation

The comparison of global geometric feature retrieval highlights the advantages of our geometric feature representation method. To further validate the effectiveness of our feature region retrieval approach, we conducted retrieval experiments on three segmented regions: flange, spoke, and rim. Fig. 7 compares the global geometric feature retrieval results with those of each segmented region. For the core part retrieval, the similarity assessment mainly relies on the length of the geometric feature image of the wheel core (i.e., the radius of the wheel core). Since the retrieval strategy and assessment method for the wheel core part are clear and intuitive, they will not be validated here.

The localized retrieval results for the flange part indicate that models W5, W35, and W84 are highly similar in the localized region. However, despite the similarity in local flange details, these models differ significantly in overall appearance from the query model. This difference underscores the diversity in flange design, providing designers with a wider range of options for reusing this part.

In the spoke section, the W46 model, which differs more in spoke structure from the query model, not appear in top 8, while the more similar W78 model ranks higher. Although the W78 model has a narrower spoke section, it shares the same number of spokes and exhibits a structure more similar to that of the query model. Additionally, similar to the W39 model in the global feature retrieval results and the W19 model in the spoke-specific retrieval results,

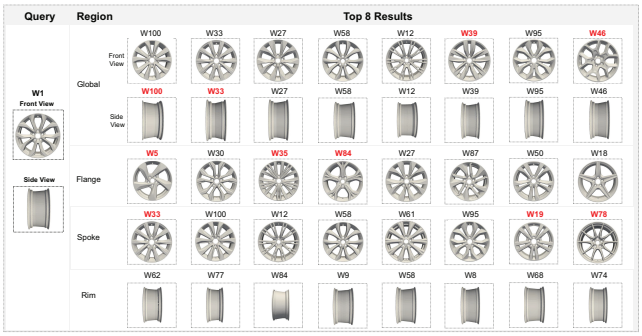

Fig. 7 Comparison of the Global Feature Retrieval Method in This Paper with the Retrieval Results of Flange, Spoke, and Rim Features. The numbered in red means the models with significant retrieval differences.

wheels with the same number of spokes but larger structural differences from the query model rank lower.

For the rim section, a comparison was made with the side view of the global feature retrieval results to more clearly visualize the differences in rim design. The side view shows that models such as W100 and W33 feature a protruding design in their rim structure, whereas the rim of the query model displays a more rounded shape without any noticeable protrusion.

In summary, local feature retrieval significantly refines search results compared to global feature retrieval. However, it does not fully allow 'on-demand' retrieval, as it relies solely on fixed, predefined regions. To enhance this process, we designed an interactive experiment allowing users to customize the selection of local features.

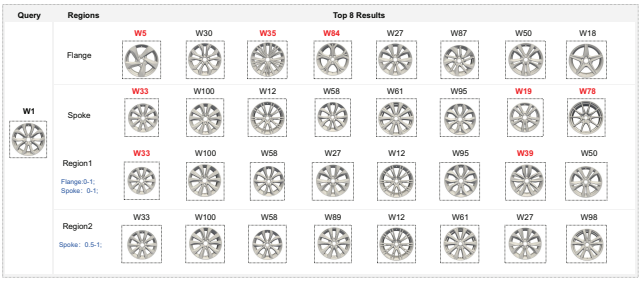

Fig. 8 Comparison of Selected Regions Retrieval Results. The customized selection retrieval results are compared with the corresponding flange and spoke local feature retrieval results. Region1 is 0%-100% of the flange part and 0%-100% of the spoke part. Region2 is 50%-100% of the spoke part.

In the customized retrieval process, cross-region retrieval (0% to 100% of the flange and spoke regions, referred to as selection1) and small percentage selection within the same region (50% to 100% of the spoke region, referred to as selection2) were used as input criteria. The retrieval results are shown in Fig. 8. Region1 results show a significant improvement over the flange section's single local feature retrieval. In flange retrieval, models such as W5 and W35, which differ structurally from the query model W1, no longer top the ranking. Instead, models like W33, structurally similar to W1, are prioritized. In Region2 retrieval, model W12, with bifurcations at the end of the spoke, shows a lower ranking than the overall spoke portion retrieval. Similarly, models like W19 and W78, which significantly differ from the query model in spoke structure, also experience ranking declines.

In summary, our method shows minimal difference from the UV-Net method in global geometric feature retrieval. Distinguishing fine-grained feature differences in global geometric features is challenging. However, our method, which allows users to select feature regions, effectively supports fine-grained feature retrieval for wheel models. Moreover, it enhances interpretability by linking feature inputs with retrieval results through geometric feature image analysis.

4.2 User Evaluation on Wheel Dataset

In this section, we further evaluate the operability and comprehensibility of our framework through experiments and interviews with thirteen domain experts (D1 to D13).

4.2.1 Evaluation of Geometric Feature Comparisons

For the comparative evaluation of global geometric features, we selected 8 3DWM models with highly similar shapes but different local features, as identified by domain expert D1. The remaining experts were divided into two groups for four experiments. In the first experiment, two models were compared; in the second, four models; in the third, six models; and in the fourth, eight models. Experts ranked the size, thickness, and spoke hole of each model, and we recorded the completion times. One group (D2, D3, D6, D7, D10, D11) used commonly employed design software, while the other group (D4, D5, D8, D9, D12, D13) used our geometric feature images. To ensure experiment accuracy, both groups began each comparison with the same software initialization state.

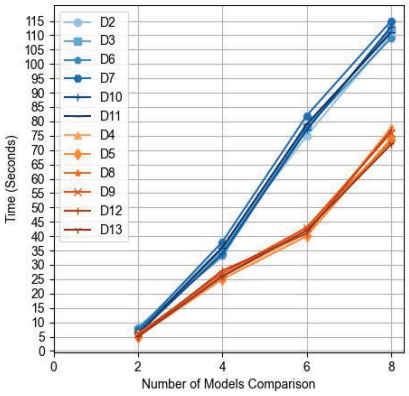

Fig. 9 Comparison of Experimental Data Between Two Groups. The blue line represents Group 1, and the orange line represents Group 2.

Fig. 9 presents the recorded experimental data results. The results show little difference in the time taken by the two groups when comparing two models. However, a time difference appears when comparing four models. For six and eight models, domain experts using our geometric feature images completed the tasks in the shortest time. These results demonstrate that our method effectively characterizes both global and local geometric features of 3DWM, facilitating easier understanding and identification of key features by users.

4.2.2 User Interview on Interactive Retrieval

We invited thirteen domain experts to evaluate our framework, focusing on its usability, comprehensibility, and potential improvements. All experts have extensive knowledge in wheel product design and a particular interest in similarity model retrieval. We initially spent 20 minutes introducing the key technologies and visual interfaces within the retrieval framework. The experts actively participated in discussions on the framework's requirements and features, quickly becoming familiar with the system's functions. We then presented two search cases to the experts and gave them 30 minutes to explore the system freely. Afterward, we held face-to-face discussions to gather their feedback and insights.

All experts agreed that the framework presented in this study strongly supports 3DWM retrieval, with customized geometric feature region selection enhancing the understanding of retrieval results and contributing to more effective design information referencing. Expert D1 emphasized that the design of geometric feature images allows users to quickly and accurately capture 3DWM features. Expert D2 suggested adding a region scaling display function to complement the current geometric feature images, which would enhance local feature comparison. Experts D3 and D4 noted that the custom background design for the selection region helped clarify the relationship between geometric features and retrieval results. Expert D5 highlighted that the ability to quickly select segmented feature regions enhances feature comparison tasks and improves retrieval efficiency. Expert D7 recommended adding an option to visualize hierarchical feature comparisons, allowing users to refine their search results based on feature categories. Expert D13 emphasized the importance of user customization, suggesting that users should be able to save their preferred settings for future retrieval tasks. All experts agree that the system demonstrates high comprehensibility, particularly in the feature correspondence between the retrieval model and its results.

In response to the suggestions from experts D7 and D13, a retrieval option in the results has been designed in the system for enterprise application scenarios. This option allows users to perform hierarchical feature retrieval and gradually refine the retrieval scope. Additionally, the system incorporates a button to save the current selections, enabling users to review valid search settings. In practical use, users have reported that these functions are convenient and user-friendly.

4.3 Experiment on ModelNet40

ModelNet40 [55], a widely used benchmark dataset, provides a diverse set of 3D models for evaluating retrieval algorithms. It contains CAD models from the 40 categories. We evaluate our geometric feature representation method based on the test set of the ModelNet40 dataset. Since our method does not rely on training data, we directly extract geometric features from the models in the test set and perform similarity calculations. To assess the sensitivity of our method in shape retrieval, we did not adjust the pose of the models in the test set but only applied uniform scaling to the model sizes for feature extraction.

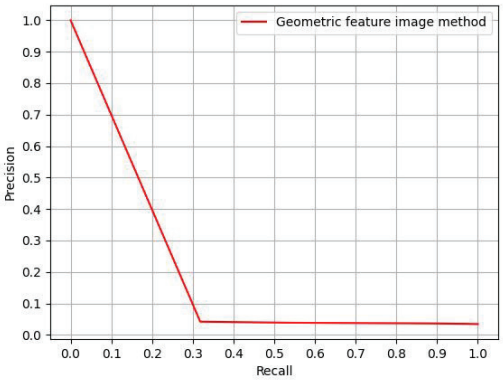

Fig. 10 PR Curve Based on Geometric Feature Extraction Method.

Fig. 10 shows the PR curve for model retrieval based on geomet-

ric feature extraction method. The shape of the PR curve reflects the performance of the model. The closer the curve is to the upper-right corner, the better the model's performance, indicating high precision and recall. Based on the PR curve, the method proposed in this paper demonstrates relatively poor retrieval accuracy.

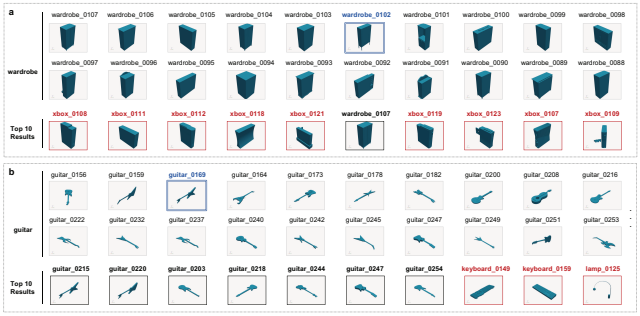

Fig. 11 TOP 10 retrieval results for Wardrobe_0102 (a) and Guitar_0169 (b). The retrieval results are sorted in descending order from left to right.

Are the retrieval results accurate? We carefully examined the Top 10 retrieval results for each object and observed an interesting phenomenon. Fig. 11 presents two representative retrieval results. In Fig. 11 (a), we show all models in the 'wardrobe' category from the dataset, along with the Top 10 retrieval results for wardrobe_0102. Among the retrieval results, wardrobe_0107 belongs to the 'wardrobe' category and shares a similar structure with wardrobe_0102, featuring four legs. However, the remaining nine results belong to different categories, yet these nine models are structurally more similar to wardrobe_0102 in terms of width and height than to other models in their respective categories. The similarity value of xbox_0109 is 0.56, which might explain the larger structural difference observed. In Fig. 11 (b), we show 20 models from the 'guitar' category and the Top 10 retrieval results for guitar_0169. Among the results, guitar_0215 and guitar_0220 share a similar structural form and detailed features with guitar_0169. The other guitar models exhibit consistent structural forms, indicating high similarity in geometric features. However, three results from categories other than 'guitar' have similarity values close to each other, but their structures differ from the retrieved model. These results suggest that the geometric feature representation method in this paper performs well for retrieving models with highly similar geometries and consistent poses. However, when retrieving from different categories, there can be situations where models from different categories exhibit similar geometric features, leading to potential errors.

4.4 Limitations

Our retrieval framework has certain limitations. First, geometric features are not suitable for capturing small geometric differences. The geometric feature mapping scheme designed in this paper is based on design shapes and does not account for geometric differences smaller than 1mm. Second, the geometric feature visualization method is suitable for 3D models with highly similar structural shapes. Due to the high global similarity features of 3DWM, when applied to models from other categories or those with large pose differences, our method may produce certain similarity calculation errors. This is because the method relies on the similarity of geometric feature images, and errors are more likely to occur when the structural differences between 3D models are large but their geometric feature images remain similar. This limitation makes our method more applicable to 3D models with similar structural shapes, such as wheel models and gear models. Third, the geometric feature segmentation method also has limitations. The geometric feature segmentation method proposed in this paper is suitable for segmenting features of models with highly similar structural shapes. When there are significant shape differences between models, segmentation of the geometric feature images may lead to uncontrollable sequence length matching, thus complicating the similarity comparison. Finally, the retrieval time and complexity of the method presented in this paper are influenced by the retrieval conditions selected by the user. When the user selects fewer retrieval conditions, the retrieval efficiency is higher; however, as more feature areas are selected, the retrieval efficiency gradually decreases.

5 Conclusion

To address the challenges of reusing 3DWM information in retrieval, this paper proposes an interactive retrieval framework based on geometric feature images for user-selected geometric feature regions. First, to accurately capture the key geometric features of 3DWM, a global geometric feature visualization method based on axial rotation model intersection is designed. The geometric feature images generated by this method encompass the size, thickness, and shape structure of the 3DWM, providing a visual representation of the model's global geometric features. Second, based on geometric feature images and the design characteristics of 3DWM models, an interactive method is developed that allows users to define segmented region features and select comparative features flexibly through customizable multi-local geometric feature combination descriptors. Third, a similarity calculation method tailored for the interactive framework is proposed, leveraging geometric feature images and custom combination feature descriptors to ensure the interpretability of the relationship between retrieval results and the corresponding retrieval features. To validate the effectiveness of the proposed method, experiments and user evaluations were conducted on real industrial datasets. The results demonstrate that this method outperforms traditional global shape retrieval methods, particularly user-centered visual interactive retrieval methods, offering greater flexibility and interpretability in practical applications and providing more accurate and efficient tools for 3DWM retrieval and information reuse.

In future work, we will focus on adaptive geometric feature visualization and multimodal representation. Our current rotation sampling feature extraction method uses a fixed step size (i.e., during the rotation sampling process, the wheels rotate by the same angle at each step), leading to sparse sampling points near the center, which may introduce similarity calculation errors. Therefore, enhancing the sampling density in feature-rich regions is a key region of focus. Additionally, we aim to integrate multimodal CAD information (such as label data) to further enhance the accuracy of retrieval models. Furthermore, we will optimize the geometric feature representation method to expand its applicability to a broader range of model categories, thereby improving the universality and accuracy of the method.

6 Acknowledgments

This work was supported in part by grants from the National Science Foundation of China (Grant no. 61802334), the Natural Science Foundation of Hebei Province (F2022203015, F2025203008), and the Innovation Capability Improvement Plan Project of Hebei Province (22567637H).

References

[1] Ji, X., & Abdoli, S. (2023). Challenges and opportunities in product life cycle management in the context of industry 4.0. Procedia CIRP, 119, 29-34. 1

[2] Klose, S. A., & Fröhling, M. (2025). A new circular economy conception for sustainable product design. Journal of Industrial Ecology, 546–560. 1

[3] Iyer, N., Jayanti, S., Lou, K., Kalyanaraman, Y., & Ramani, K. (2005). Three-dimensional shape searching: state-of-the-art review and future trends. Computer-Aided Design, 37(5), 509-530. 1

[4] Ji, B., Zhang, J., Li, Y., & Pang, J. (2023). Free-form CAD model retrieval approach for engineering reuse based on local feature segmentation. Computers & Graphics, 111, 111-121. 1

[5] Tam, G. K., & Lau, R. W. (2024). Deformable model retrieval based on topological and geometric signatures. IEEE transactions on visualization and computer graphics, 13(3), 470-482. 2

[6] Mohamed, H. H., Belaid, S., Naanaa, W., & Romdhane, L. B. (2021). Deep sparse dictionary-based representation for 3D non-rigid shape retrieval. In Proceedings of the 36th Annual ACM Symposium on Applied Computing, pp. 1070-1077. 2

[7] Shih, J. L., Lee, C. H., & Wang, J. T. (2007). A new 3D model retrieval approach based on the elevation descriptor. Pattern Recognition, 40(1), 283-295. 2

[8] Chen, D. Y., Tian, X. P., Shen, Y. T., & Ouhyoung, M. (2003). On visual similarity based 3D model retrieval. In Computer graphics forum, pp. 223-232. Oxford, UK: Blackwell Publishing, Inc. 2

[9] Gao, Z., Li, Y., & Wan, S. (2020). Exploring deep learning for view-based 3D model retrieval. ACM transactions on multimedia computing, communications, and applications (TOMM), 16(1), 1-21. 2

[10] Guo, H., Wang, J., Gao, Y., Li, J., & Lu, H. (2016). Multi-view 3D object retrieval with deep embedding network. IEEE Transactions on Image Processing, 25(12), 5526-5537. 2

[11] Manda, B., Dhayarkar, S., Mitheran, S., Viekash, V. K., & Muthuganapathy, R. (2021). 'CADSketchNet'-An annotated sketch dataset for 3D CAD model retrieval with deep neural networks. Computers & Graphics, 99, 100-113. 2

[12] Fu, X., Song, D., Yang, Y., Zhang, Y., & Wang, B. (2025). S2Mix: Style and Semantic Mix for cross-domain 3D model retrieval. Journal of Visual Communication and Image Representation, 107, 104390. 2

[13] LeCun, Y., Bengio, Y., & Hinton, G. (2015). Deep learning. nature, 521(7553), 436-444. 2

[14] Li, G., Wang, J., Wang, Y., Shan, G., & Zhao, Y. (2023). An in-situ visual analytics framework for deep neural networks. IEEE Transactions on Visualization and Computer Graphics, 30(10), 6770-6786. 2

[15] Wang, J., Liu, S., & Zhang, W. (2024). Visual analytics for machine learning: A data perspective survey. IEEE transactions on visualization and computer graphics, 30(12), 7637-7656. 2

[16] Saupe, D., & Vranić, D. V. (2001, September). 3D model retrieval with spherical harmonics and moments. In Joint Pattern Recognition Symposium, pp. 392-397. Berlin, Heidelberg: Springer Berlin Heidelberg. 2

[17] Qin, Z., Jia, J., & Qin, J. (2008, June). Content based 3D model retrieval: A survey. In 2008 International Workshop on Content-Based Multimedia Indexing, pp. 249-256. IEEE. 2

[18] Akgül, C. B., Sankur, B., Yemez, Y., & Schmitt, F. (2009). 3D model retrieval using probability density-based shape descriptors. IEEE transactions on pattern analysis and machine intelligence, 31(6), 1117-1133. 2

[19] Bai, J., Gao, S., Tang, W., Liu, Y., & Guo, S. (2010). Design reuse oriented partial retrieval of CAD models. Computer-Aided Design, 42(12), 1069-1084. 2, 3

[20] Herzog, V., & Suwelack, S. (2023). Bridging the Gap between geometry and user intent: retrieval of CAD models via regions of interest. Computer-aided design, 163, 103573. 2

[21] Li, Y., Zhang, J., Pang, J., & Yao, Y. (2025). Harnessing unsupervised learning for retrieving CAD assembly models from public datasets. Advanced Engineering Informatics, 65, 103182. 2

[22] Qi, A., Gryaditskaya, Y., Song, J., Yang, Y., Qi, Y., Hospedales, T. M., ... & Song, Y. Z. (2021). Toward fine-grained sketch-based 3D shape retrieval. IEEE transactions on image processing, 30, 8595-8606. 2

[23] Min, P., Kazhdan, M., & Funkhouser, T. (2004). A comparison of text and shape matching for retrieval of online 3D models. In Research and Advanced Technology for Digital Libraries: 8th European Conference, ECDL 2004, Bath, UK, September 12-17, 2004. Proceedings 8, pp. 209-220. Springer Berlin Heidelberg. 2

[24] Yang, Y., Lin, H., & Zhang, Y. (2007). Content-based 3-D model retrieval: A survey. IEEE Transactions on Systems, Man, and Cybernetics, Part C (Applications and Reviews), 37(6), 1081-1098. 2

[25] Osada, R., Funkhouser, T., Chazelle, B., & Dobkin, D. (2002). Shape distributions. ACM Transactions on Graphics (TOG), 21(4), 807-832. 2

[26] Lian, Z., Godil, A., Bustos, B., Daoudi, M., Hermans, J., Kawamura, S., ... & Suetens, P. D. (2011). Shape retrieval on non-rigid 3D watertight meshes. In Eurographics workshop on 3d object retrieval (3DOR), 1-12. 2

[27] Pickup, D., Sun, X., Rosin, P. L., Martin, R. R., Cheng, Z., Lian, Z., ... & Ye, J. (2016). Shape retrieval of non-rigid 3d human models. International Journal of Computer Vision, 120, 169-193. 2

[28] Schmitt, W., Sotomayor, J. L., Telea, A., Silva, C. T., & Comba, J. L. (2015, August). A 3D shape descriptor based on depth complexity and thickness histograms. In 2015 28th SIBGRAPI Conference on Graphics, Patterns and Images, pp. 226-233. IEEE. 2

[29] Vranic, D. V., Saupe, D., & Richter, J. (2001). Tools for 3D-object retrieval: Karhunen-Loeve transform and spherical harmonics. In 2001 IEEE Fourth Workshop on Multimedia Signal Processing, pp. 293-298. IEEE. 2

[30] Youssef, C. (2016). Spatiotemporal representation of 3d skeleton joints-based action recognition using modified spherical harmonics. Pattern Recognition Letters, 83, 32-41. 2

[31] Jallouli, M., Khalifa, W. B. H., Mabrouk, A. B., & Mahjoub, M. A. (2018). Spherical harmonics entropy for optimal 3D modeling. arXiv preprint arXiv:1805.08084. 2

[32] Mademlis, A., Daras, P., Tzovaras, D., & Strintzis, M. G. (2009). Ellipsoidal harmonics for 3-D shape description and retrieval. IEEE transactions on multimedia, 11(8), 1422-1433. 2

[33] Hilaga, M., Shinagawa, Y., Kohmura, T., & Kunii, T. L. (2001). Topology matching for fully automatic similarity estimation of 3D shapes. In Proceedings of the 28th annual conference on Computer graphics and interactive techniques, pp. 203-212. 3

[34] Sirin, Y., & Demirci, M. F. (2017). 2D and 3D shape retrieval using skeleton filling rate. Multimedia Tools and Applications, 76, 7823-7848. 3

[35] Maturana, D., & Scherer, S. (2015, September). Voxnet: A 3d convolutional neural network for real-time object recognition. In 2015 IEEE/RSJ international conference on intelligent robots and systems (IROS), pp. 922-928. IEEE. 3

[36] Chang, J., Zhang, L., & Shao, Z. (2023). View-target relation-guided unsupervised 2D image-based 3D model retrieval via transformer. Multimedia Systems, 29(6), 3891-3901. 3

[37] Yeo, C., Cheon, S. U., Lim, S., Park, J. H., & Mun, D. (2024). Relational descriptors for retrieving design features in a B-rep model using the similarity-based retrieval approach. Advanced Engineering Informatics, 62, 102877. 3

[38] Wu, Z., Song, S., Khosla, A., Yu, F., Zhang, L., Tang, X., & Xiao, J. (2015). 3d shapenets: A deep representation for volumetric shapes. In Proceedings of the IEEE conference on computer vision and pattern recognition, pp. 1912-1920. 3

[39] Hinton, G. E., Osindero, S., & Teh, Y. W. (2006). A fast learning algorithm for deep belief nets. Neural computation, 18(7), 1527-1554. 3

[40] Lin, C., Wang, P., Xiong, S., & Chen, R. (2024). Orthogonal integral transform for 3D shape recognition with few examples. The Visual Computer, 40(5), 3271-3284. 3

[41] Qi, C. R., Su, H., Mo, K., & Guibas, L. J. (2017). Pointnet: Deep learning on point sets for 3d classification and segmentation. In Proceedings of the IEEE conference on computer vision and pattern recognition, pp. 652-660. 3

[42] Su, H., Maji, S., Kalogerakis, E., & Learned-Miller, E. (2015). Multi-view convolutional neural networks for 3d shape recognition. In Proceedings of the IEEE international conference on computer vision, pp. 945-953. 3

[43] Feng, Y., Zhang, Z., Zhao, X., Ji, R., & Gao, Y. (2018). Gvcnn: Group-view convolutional neural networks for 3d shape recognition. In Proceedings of the IEEE conference on computer vision and pat-

tern recognition, pp. 264-272. 3

[44] Tang, K., Chen, Y., Peng, W., Zhang, Y., Fang, M., Wang, Z., & Song, P. (2023). Reppvconv: attentively fusing reparameterized voxel features for efficient 3d point cloud perception. The Visual Computer, 39(11), 5577-5588. 3

[45] Liang, Q., Wang, Y., Nie, W., & Li, Q. (2020). MVCLN: multi-view convolutional LSTM network for cross-media 3D shape recognition. IEEE Access, 8, 139792-139802. 3

[46] Colligan, A. R., Robinson, T. T., Nolan, D. C., Hua, Y., & Cao, W. (2022). Hierarchical cadnet: Learning from b-reps for machining feature recognition. Computer-Aided Design, 147, 103226. 3

[47] Hou, J., Luo, C., Qin, F., Shao, Y., & Chen, X. (2023). FuS-GCN: Efficient B-rep based graph convolutional networks for 3D-CAD model classification and retrieval. Advanced Engineering Informatics, 56, 102008. 3, 7

[48] Bespalov, D., Regli, W. C., & Shokoufandeh, A. (2006). Local feature extraction and matching partial objects. Computer-Aided Design, 38(9), 1020-1037. 3

[49] Biasotti, S., Marini, S., Spagnuolo, M., & Falcidieno, B. (2006). Sub-part correspondence by structural descriptors of 3D shapes. Computer-Aided Design, 38(9), 1002-1019. 3

[50] Bai, J., Liu, Y., & Gao, S. (2007, October). Multi-mode solid model retrieval based on partial matching. In 2007 10th IEEE international conference on computer-aided design and computer graphics, pp. 126-131. IEEE. 3

[51] Persoon, E., & Fu, K. S. (2007). Shape discrimination using Fourier descriptors. IEEE Transactions on systems, man, and cybernetics, 7(3), 170-179. 7

[52] Jayaraman, P. K., Sanghi, A., Lambourne, J. G., Willis, K. D., Davies, T., Shayani, H., & Morris, N. (2021). Uv-net: Learning from boundary representations. In Proceedings of the IEEE/CVF conference on computer vision and pattern recognition, pp. 11703-11712. 3, 7

[53] Jayanti, S., Kalyanaraman, Y., Iyer, N., & Ramani, K. (2006). Developing an engineering shape benchmark for CAD models. Computer-Aided Design, 38(9), 939-953. 7

[54] Dekhtiar, J., Durupt, A., Bricogne, M., Eynard, B., Rowson, H., & Kiritsis, D. (2018). Deep learning for big data applications in CAD and PLM–Research review, opportunities and case study. Computers in Industry, 100, 227-243. 7

[55] Wu, Z., Song, S., Khosla, A., Yu, F., Zhang, L., Tang, X., & Xiao, J. (2015). 3d shapenets: A deep representation for volumetric shapes. In Proceedings of the IEEE conference on computer vision and pattern recognition, pp. 1912-1920. 9